Microstructural design of hardfacing Ni-Cr-B-Si-C alloys

Hemmati, I.; Huizenga, R. M.; Ocelik, V.; De Hosson, J. Th M.

Published in:
Acta Materialia

DOI:
10.1016/j.actamat.2013.06.048

Publication date:
2013

Available online at www.sciencedirect.com

SciVerse ScienceDirect

Acta Materialia 61 (2013) 6061–6070

Acta MATERIALIA

www.elsevier.com/locate/actamat

Microstructural design of hardfacing Ni–Cr–B–Si–C alloys

I. Hemmati [a], R.M. Huizenga [b], V. Ocelík [a,*], J.Th.M. De Hosson [a]

[a] Materials innovation institute (M2i), Department of Applied Physics, University of Groningen, Nijenborgh 4, Groningen 9474 AG, The Netherlands
[b] Department of Materials Science and Engineering, Delft University of Technology, Mekelweg 2, Delft 2628 CD, The Netherlands

Received 16 April 2013; received in revised form 19 June 2013; accepted 25 June 2013
Available online 23 July 2013

Abstract

This work reports the procedure for selection of alloying elements to refine the microstructure of hardfacing Ni–Cr–B–Si–C alloys by providing in situ formed nucleation agents. It is concluded that the refining element should be able to spontaneously produce precipitates at high temperatures with little solubility in their Cr-rich counterparts. After exploring the theoretical backgrounds on how to select the refining element, Nb and Zr were selected and the phase formation reactions of Zr- or Nb-modified Ni–Cr–B–Si–C alloys were calculated using Thermo-Calc® simulations. Detailed microstructural analyses of the rapidly solidified samples deposited from the modified alloys showed that addition of Nb in specific quantities induces a significant microstructural refinement in the original Ni–Cr–B–Si–C alloy without deteriorating its high hardness. The Nb-modified alloy could be used to further investigate the viability of microstructural refinement as an effective toughening mechanism for Ni–Cr–B–Si–C and similar alloy systems.

Keywords: Microstructural refinement; Analytical electron microscopy; Nickel alloys; Nucleation; Laser deposition

1. Introduction

Ni-base hardfacing alloys such as the Ni–Cr–B–Si–C family are used in applications where a combination of surface wear and corrosion resistance is required [1]. In recent years, laser deposition technologies have been increasingly used to produce dense Ni–Cr–B–Si–C coatings with metallurgical bonding to the substrate and superior functional properties [2–4]. However, a major drawback for laser deposition of these alloys is their high cracking susceptibility under the rapid cooling rates of the laser processing [5]. There has been a number of attempts to solve the cracking problem of Ni–Cr–B–Si–C alloys by either reducing the cooling rate of the deposits using preheating and postheating [6–8] or increasing the toughness of the alloys by compositional modification [5,6,9,10]. The latter approach, which is more attractive from the practical and economic perspectives, has been concentrated on eliminating or refining the large Cr boride and carbide precipitates by the addition of early transition metals (ETMs) such as titanium (Ti) [9], vanadium (V) [5,6] or tantalum (Ta) [10].

Toughening of Ni–Cr–B–Si–C alloys by eliminating large Cr-rich precipitates is based on the observation of crack growth in their microstructures. It was shown that Cr borides and carbides such as CrB, Cr_5B_3 or Cr_7C_3 act as sites for crack nucleation, as well as being easy routes for crack growth [5,6,11]. The maximum stress (σ_m) concentrated at the tip of an individual fractured Cr-rich precipitate can be described by the classical formulation as

$$\sigma_m = 2\sigma_a\sqrt{a/\rho_c}$$

where σ_a is the applied stress, ρ_c is the radius of curvature for crack tip and a is the length of the crack, i.e. the size of the precipitate [12]. Improvements in cracking susceptibility of the deposits are expected with more refined precipitates, i.e. smaller a. Such an improvement in the toughness of rather brittle materials by decreasing the structural scale of the strengthening precipitates has been reported for Fe-base hardfacing alloys, in which refinement

* Corresponding author. Tel.: +31 503633407.
E-mail address: v.ocelik@rug.nl (V. Ocelík).

1359-6454/$36.00
http://dx.doi.org/10.1016/j.actamat.2013.06.048

of borocarbide phases substantially improved the toughness while preserving the original level of hardness [13].

One way to refine the Cr boride and carbide precipitates is to provide them with nucleation sites formed in situ during solidification. New boride or carbide precipitates forming at higher temperatures can be good candidates for nucleation sites. It has been previously suggested that the criterion to select the refining element for Ni–Cr–B–Si–C alloys is that the element should have a high affinity for B or C [9,10], i.e. the Gibbs free energy of formation (ΔG_f) for borides or carbides of that element should be more negative than those of Cr-rich precipitates [5]. Although spontaneous formation (negative ΔG_f) is a prerequisite for formation of nucleating sites, the lack of microstructural refinement in the Ni–Cr–B–Si–C deposits modified by V [5,6], Ti [9] or Ta [10] raises the question of whether factors other than affinity for B or C play a role in the refinement process.

In our previous work [6], Colmonoy 69 alloy powder (nominal composition: Ni–13.5Cr–3B–4Si–0.7C–2.1Mo–1.7Cu–4Fe (wt.%)) modified by different contents of vanadium was deposited by laser cladding. The reason for selecting vanadium was that its borides have some of the largest negative values of ΔG_f and hence are likely to precipitate out preferentially in comparison to Cr borides [14]. In fact, vanadium addition is a good way to check the idea of selecting a refining element according to the ΔG_f criterion alone. However, the addition of vanadium did not induce considerable microstructural refinement in laser-deposited Ni–Cr–B–Si–C coatings. Instead, the morphology and nature of the boride phases were changed (from blocky to rod shaped), and VC precipitates were added to the microstructure [6].

In the V-modified system, VB did not remain as an independent phase. Instead, it went into solid solution with the more abundant CrB and created (Cr,V)B precipitates. On the other hand, VC existed as an independent phase because VC and Cr_7C_3 do not dissolve in each other as a result of their different crystal structures [6]. The V-modified system showed that, to select an effective refining element for the intended alloy system, not only should the capability of the element to spontaneously form boride or carbide phases be considered, but its compounds should also have limited solid solubility in their Cr-rich counterparts.

In this study, two new alloying elements, Nb and Zr, were selected after exploring the theoretical backgrounds on effective refining elements for this alloy system. The main purpose of the current work is to investigate the underlying ideas of how to choose an alloying element for microstructural refinement of precipitation-strengthened hardfacing alloys such as Ni–Cr–B–Si–C. In this way, a set of generic criteria can be defined that an element should fulfill to produce nucleating agents with the ultimate goal of enhancing the toughness of the intended alloys through microstructural refinement.

2. Theoretical backgrounds

In this section, a number of rules will be defined for the selection of potential refining elements for Ni–Cr–B–Si–C alloys. The ideas and the procedure could also be applied to produce in situ formed nucleation agents in similar alloy systems. As Ni–Cr–B–Si–C alloys have substantial contents of boron and carbon, in situ formed borides or carbides can be good candidates for heterogeneous nucleation sites. In order to find potential refining elements, the focus will be on ETMs, as most of them are strong boride and carbide formers [15–17]. Based on the outcome of our previous research on the addition of vanadium [6] as well as the results published by others [9,10], a refining element for the intended alloy system should fulfill at least the following three criteria, which will be subsequently elaborated and applied to find potential candidate ETM refining elements:

(i) The affinity of the refining element for B or C should be higher than the affinity of Cr for these elements, i.e. it should have the possibility of preferential formation of borides or carbides during solidification.
(ii) The boride or carbide precipitates of the refining element should have limited solid solubility in their Cr-rich counterparts.
(iii) The boride or carbide precipitates of the refining element should form at a higher temperature in comparison to Cr-rich precipitates.

2.1. Affinity for carbon and boron

The affinity of ETMs for C is highest for a valence number of 4 and decreases for higher valences, as explained by Cottrell [15]. According to Table 1, Ti, Zr and Hf should have the highest affinities for C. In addition, Ta and Nb should be stronger carbide formers than Cr. The data on heats of formation (ΔH) and ΔG_f of carbides such as ZrC, TiC, HfC and NbC confirm such predictions [14,15]. Similarly, the affinities of Ti, Zr, Nb and Hf for boron are stronger than that of Cr [14,17].

2.2. Solid solubility in Cr-rich precipitates

If a solid solution forms between Cr borides/carbides and the boride/carbides of other ETMs, the ETM atoms will substitute Cr, as was observed for the case of V addition [6]. Hume–Rothery rules for substitutional solid solutions (including size, electronegativity and valence or the electron concentration factors [18]) and their derivatives, such as the methods developed by Darken and Gurry [19] and Chelikowsky [20], could be used as guidelines for judging the extent of solid solubility [21].

The difference in electronegativity between Cr and the rest of the ETMs is less than 0.4, as presented in Table 1. Hence, according to the Darken–Gurry criteria [21], elec-

Table 1
Properties of the ETMs of groups IV–VI and their size factors in comparison to Cr [16].

Element	Atomic radius (nm)	Size factor (%)	Electron configuration	Electronegativity	Most common valence
Cr	0.126	–	[Ar] $3d^5 4s^1$	1.6	6
V	0.133	5.5	[Ar] $3d^3 4s^2$	1.6	5
Ti	0.146	15.8	[Ar] $3d^2 4s^2$	1.5	4
Mo	0.138	9.5	[Kr] $4d^5 5s^1$	1.8	6
Nb	0.145	15	[Kr] $4d^4 5s^1$	1.6	5
Zr	0.159	26.1	[Kr] $4d^2 5s^2$	1.4	4
W	0.139	10.3	[Xe] $4f^{14} 5d^4 6s^2$	1.7	6
Ta	0.145	15	[Xe] $4f^{14} 5d^3 6s^2$	1.5	5
Hf	0.158	25.3	[Xe] $4f^{14} 5d^2 6s^2$	1.3	4

tronegativity will play a negligible role in determining the level of solid solubility when Cr and the other ETMs are substituted in each other's compounds. The valences of transition metals are variable and complex and, due to the valence complication caused by partially filled *d* orbitals, the transition metal alloys generally do not follow the valence rule when alloyed with other transition metals [21]. As a result, atomic size seems to be the dominant factor in determining the extent of solid solubility in this case. However, the phase constitution of the V-modified system showed that the crystal structure of the phases should also be considered [6]. In other words, while the size factor for vanadium, calculated as $\Delta r_V = (r_{Cr} - r_V)/r_{Cr}$, is equal to 5.5%, which is well within the favorable range, VC and Cr_7C_3 had little solubility as a result of their different crystal structures. Hence, the similarity of the crystal structures should also be considered.

In addition to V, several other ETMs were passed over in the current work for a variety of reasons. Modification of Ni–Cr–B–Si–C alloys by Ti [9] or Ta [10] have been previously done without success. Mo and W were also skipped because neither is a strong carbide or boride former [15]. On the other hand, Zr and Hf are very strong carbide and boride formers (Table 1 and Ref. [17]), and have the most unfavorable size factors (i.e. favorable for limited solubility in Cr-rich phases). Industrial-grade Zr contains Hf as a natural impurity, so pure Hf was also skipped. Furthermore, Zr borides and carbide such as ZrB_2 and ZrC have crystal structures that are different from their Cr-rich counterparts [16,17]. Consequently, strong segregation of Cr-rich and Zr-rich precipitates is expected (as already confirmed experimentally [22]). Finally, Nb has a high affinity for boron and carbon (Table 1 and Ref. [17]) and an unfavorable size factor. Nb may form multiple borides/carbides which all have very limited solubility in their Cr-rich counterparts [23,24]. Hence, Zr- and Nb-rich precipitates are expected to remain as independent phases and provide potential nucleation sites. However, these independent phases should also precipitate out at a high enough temperature, and this will be checked in the next section.

2.3. Temperature of boride/carbide phase formation

According to the binary phase diagrams, both Zr and Nb form borides/carbides at very high temperatures (e.g. above 3000 °C). However, the temperatures of boride/carbide precipitation, especially for Zr, drop very quickly with slight compositional variations [25–27]. As a result, the phase formation reactions should be evaluated for the actual alloy. For this purpose, the sequence of phase formation reactions in the alloys modified by 5 wt.% of Zr or Nb additions were simulated using Thermo-Calc® software (version S, database TTNI version 6.3). In addition to calculations based on the lever rule, the Scheil module was employed to investigate the phase formation reactions in non-equilibrium solidification conditions based on the well-known Scheil–Gulliver model [28], with B and C as fast-diffusing elements. The results of thermodynamic calculations over the entire solidification range are shown in Fig. 1. For both Zr and Nb additions, the calculated precipitation reactions based on equilibrium and Scheil solidification models were very similar. However, predictions for low-temperature reactions, including eutectic ones (e.g. the formation of Ni_3B [29]), were different. In the case of the Zr-modified system, ZrB_2 is expected to solidify first; and for the Nb-modified deposits, NbC should form simultaneously with CrB. So, both Zr and Nb could form phases at the earliest stages of solidification which may provide heterogeneous nucleation sites for the Cr-rich precipitates. Based on the above discussions, Nb and Zr were selected as additional alloying elements for the experimental part of the work.

3. Experimental procedure

Colmonoy 69 was selected as the starting alloy powder for subsequent compositional modifications. Single and multi-track (five tracks, with 33% overlapping) coatings of Zr-modified and Nb-modified Colmonoy 69 with a thickness of 0.9–1.1 mm were deposited at a speed of 5 mm s^{-1} on 50-mm-diameter S355 low carbon steel rods using a side cladding powder injection nozzle, a fiber laser beam, and argon as the powder carrier and melt pool shielding gas. A twin-hopper powder feeder was used to simultaneously inject Colmonoy 69 and industrial grade Zr (Zr + Hf > 99 wt.%) or Colmonoy 69 and commercially pure Nb powders. In each case, the two powders were mixed in a cyclone before exiting the deposition nozzle. The Zr or Nb powder feeding rates were adjusted to provide up to 5 wt.% of Zr or Nb in the final coatings. Depos-

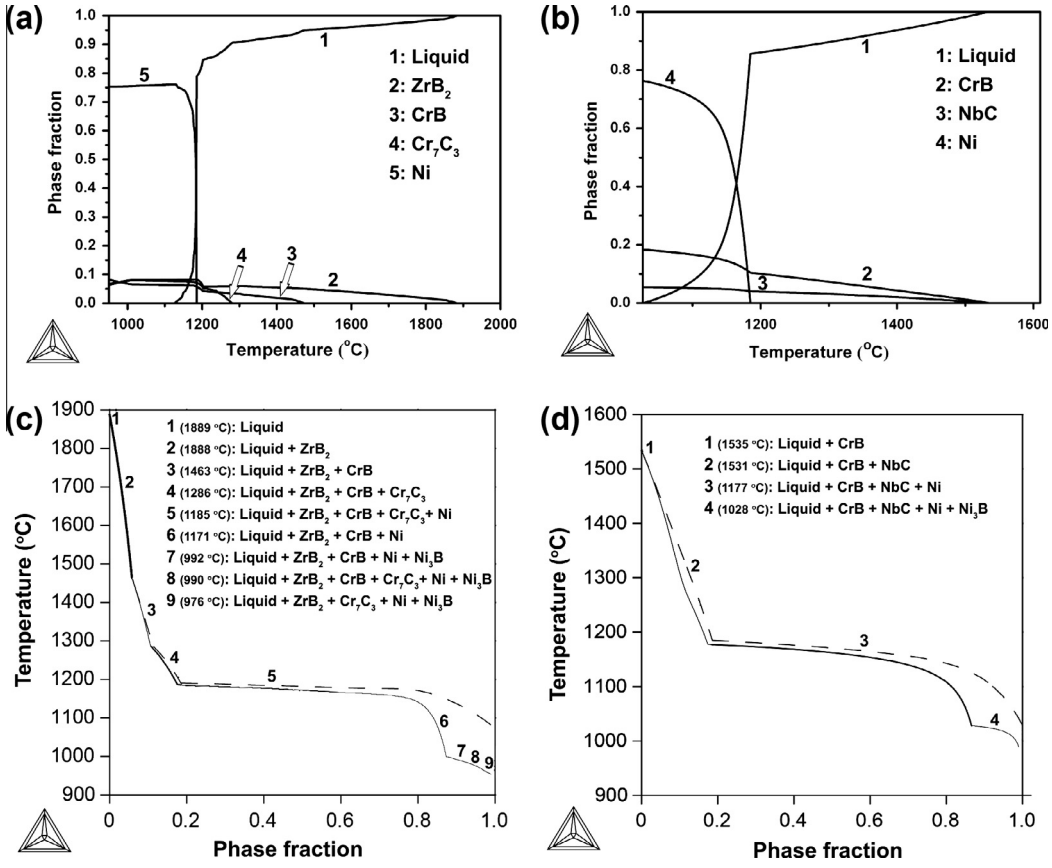

Fig. 1. Calculated equilibrium phase fraction vs. temperature for the alloys modified by (a) 5 wt.% Zr or (b) 5 wt.% Nb. (c and d) show the solidification sequence of the same alloys as in (a and b) according to the Scheil–Gulliver solidification model. The dashed lines in (c and d) show the sequence of equilibrium solidification.

its were made using a laser power of 800 W on substrates preheated to 500 °C. The preheating of the substrates was done immediately before cladding using an electric tube furnace. Dilution from the substrate [30] evaluated from optical microscopy images of transverse cross-sections was kept below 10%. In the current work, the cooling rate was kept constant by using the same set of deposition parameters. Attention was focused on the correlation between the alloy chemistry and the microstructure (and hardness) of the deposits.

Samples for further characterizations were cut and prepared by standard mechanical grinding with suspensions containing 9 and 3 μm diamond particles and polishing with colloidal Al_2O_3. A Philips XL30 field emission gun scanning electron microscope (SEM) was used for microstructural observations, mostly in backscattered electron (BSE) imaging mode. Mutual solubility of the phases was evaluated by quantitative energy-dispersive spectroscopy (EDS). To ensure the accuracy and reliability of the EDS measurements, the following steps were taken:

(i) Large precipitates were analyzed to reduce effects of the surrounding matrix.
(ii) An accelerating voltage of 5 kV was used to increase the amount of boron and carbon X-ray signals and to maximize the sensitivity of the detector for low-energy X-rays of these elements [31].
(iii) Standardless element coefficients of 4 for boron and 2 for carbon were applied in the EDAX Genesis® software to compensate for the limited detector accuracy for X-ray lines below 1 keV [29].
(iv) The halographic peak deconvolution (HPD) function in the EDAX Genesis® software was used to compare the model EDS spectra with the experimental ones to distinguish the overlap between B-K and Zr-M or B-K and Nb-M peaks.

Furthermore, a combination of EDS and electron backscatter diffraction (EBSD) was used for phase identification of the Cr-, Zr- and Nb-rich precipitates. Full details on the application of EDS/EBSD for phase identification of the boride and carbide phases in this alloy system can be found elsewhere [29]. As stated before, Thermo-Calc® simulations were used to determine the sequence and temperature of phase formation reactions. The calculated phase formations were verified against the EDS/EBSD phase identification results and simulations were repeated using a modified list of expected phases wherever necessary. The Vickers hardness of the deposits was measured at a load of 4.9 N using a Revetest® scratch testing machine.

4. Results

4.1. Microstructural observation

4.1.1. Zr-modified deposits

Fig. 2a and b shows the microstructure of samples containing 2 and 5 wt.% Zr, respectively. Lower contents of Zr mostly influenced the eutectic structure of the alloy (Fig. 2a). With more Zr additions, some Zr-rich precipitates were formed. These are visible with a bright contrast in the SEM–BSE image of Fig. 2b. It can be seen that Zr-rich particles are located at the edges of Cr boride precipitates, indicating that they were present as insoluble components and inactive particles for nucleation during solidification. In comparison to the microstructure of the original alloy [29], no appreciable microstructural refinement happened upon Zr addition.

4.1.2. Nb-modified deposits

Unlike the case of Zr addition, the microstructure of Nb-modified deposits was significantly refined, as can be seen by comparing Fig. 3a and b. Submicron Nb-rich precipitates (visible as bright particles in SEM–BSE images) acted as nucleation sites for the rod-shape phases shown in the inset of Fig. 3b. Microstructural observation of samples with different amounts of Nb additions confirmed that the refining effect of Nb was at its peak for an Nb content of around 4 wt.%. At higher Nb contents, large Nb-rich precipitates started to appear.

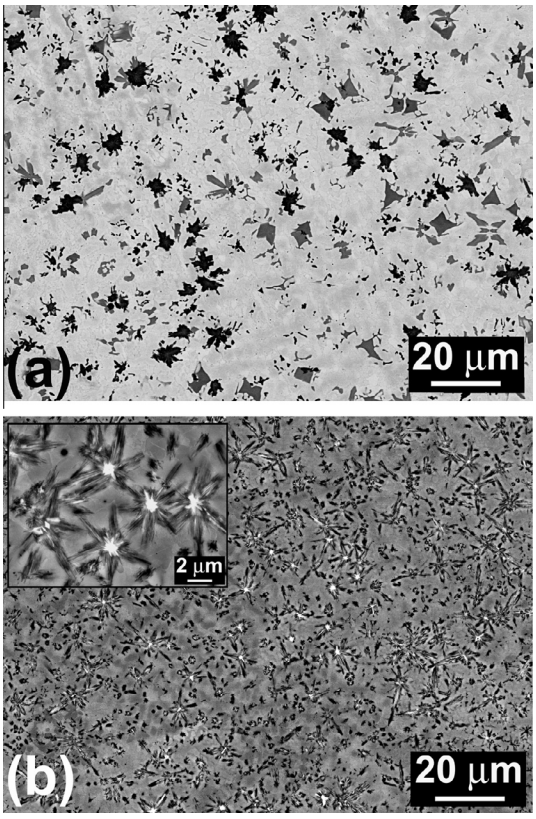

Fig. 3. SEM–BSE images comparing the microstructure of (a) Colmonoy 69 and (b) Colmonoy 69 plus 4 wt.% Nb. The inset in (b) shows the details of the refined microstructure.

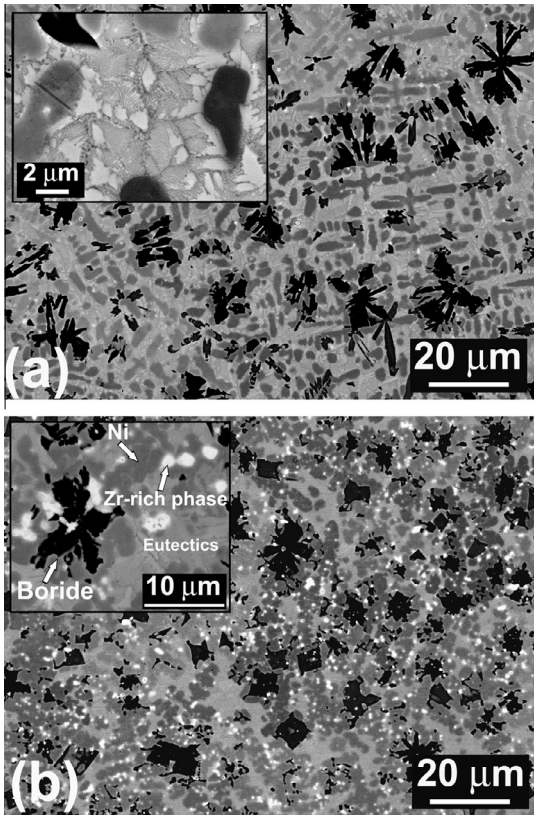

Fig. 2. SEM–BSE images showing the microstructure of Zr-modified coating containing (a) 2 wt.% and (b) 5 wt.% Zr. The insets show the details of each microstructure.

4.2. Characterization of the constituent phases

The purpose of such characterizations was twofold: first, to quantitatively determine the composition of all precipitates (Cr-rich, Zr-rich and Nb-rich), and second, to conclusively determine their type. The former could assess the mutual solubility of the phases and was performed by quantitative EDS measurements. The latter could reveal which types of phase precipitated as a result of the additional element (carbide, boride or both). For this purpose, EDS results were combined with crystallographic information from EBSD.

4.2.1. Zr-modified deposits

For EDS characterization of Zr-rich precipitates, a careful HPD has to be done because of the proximity of B-K (at 0.188 keV) and Zr-M (at 0.153 keV) characteristic X-ray lines [32]. The HPD profiles, including B-K, Zr-M and both, were generated and superimposed on the experimental EDS spectra obtained from Zr-rich precipitates. As shown in Fig. 4a, the HPD profiles confirmed that the lowest-energy peak of the spectra does not belong to B and fits

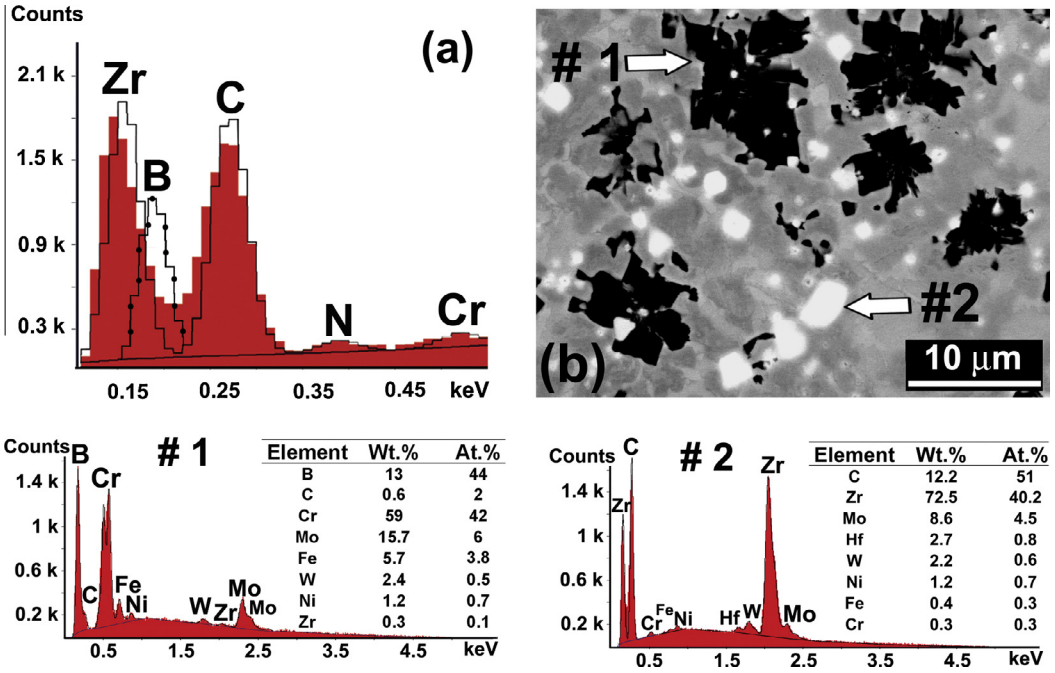

Fig. 4. (a) The HPD profile including the Zr M-line and B K-line for the EDS spectra obtained from the Zr-rich precipitates visible as bright in Fig. 2; (b) EDS quantitative analysis of Cr- and Zr-rich precipitates labeled as #1 and #2, respectively, in the SEM image.

much better to the Zr-M. As a result, the EDS peak at around 0.15 keV was assigned to Zr-M, although the Zr-L line was chosen for the quantification procedures. Afterwards, EDS spectra were obtained from the Zr- and Cr-rich precipitates shown in Fig. 4b and quantified. The ratios of Cr:B and Zr:C atomic percentages in precipitates #1 and #2 were both close to unity. Hence, they were expected to be of CrB and ZrC type, respectively (as will be confirmed by the EBSD results later).

EBSD patterns were obtained and indexed by a list of candidate phases developed from the database of the International Center for Diffraction Data (ICDD). Both Zr carbides and borides were included in the list of candidate phases. Fig. 5a shows the BSE image (tilted 70°) from the microstructure of Zr-modified deposits. The EBSD pattern of the Zr carbide precipitates (bright particles) could be precisely (with a solution error of less than 0.5°) and reproducibly indexed as ZrC, as shown in Fig. 5b. The Cr-rich precipitates (the dark phase) were indexed as CrB. Fig. 5c shows the combination of phase and image quality maps taken from the microstructure of the area shown in Fig. 5a. The formation of ZrC precipitates on CrB and the Ni dendrite arms surrounding them are clearly visible.

The map of Fig. 5c implies that the interdendritic areas consist of ZrC, which is not actually true. The interdendritic areas contain Ni plus other phases (Ni–Si–Zr type, according to EDS analyses). The submicron scale of the layers in the interdendritic eutectic structure (Fig. 2b) means that EBSD patterns could come from more than one phase at any time. This resulted in low-quality patterns, which have a Ni component in most cases. Ni and ZrC have very similar crystallographic features (both *(O_h)[m3m]* symmetry point group; lattice parameters: 0.4693 nm for ZrC (ICDD #350784) and 0.356 nm for Ni). Hence, they can be misindexed as one another. In areas with a high-quality diffraction pattern, i.e. when the signal came from ZrC or Ni dendrites, it was possible to reliably distinguish them by limiting the number of indexed bands to 10. However, in eutectic areas, diffuse Ni patterns were misindexed as ZrC but with a lower image quality, i.e. darker contrast in the image quality map (Fig. 5c).

Based on the EDS/EBSD phase identifications, the only Zr-rich precipitate in the Zr-modified alloys was ZrC and not Zr borides such as ZrB_2 as predicted by initial Thermo-Calc® simulations (Fig. 1a). As a result, it was necessary to recalculate the solidification of the Zr-modified alloy by excluding ZrB_2 from the list of possible phases. The graph of recalculated phase fractions presented in Fig. 5d precisely matches the experimental observations in terms of type and sequence of phase formation, i.e. the absence of Cr_7C_3 and the formation of ZrC at lower temperatures in comparison to CrB.

4.2.2. Nb-modified deposits

The same procedures were followed to assess the mutual solubility of boride/carbide phases in the Nb-modified deposits and to determine their type. The issues which had to be solved before proceeding with the EDS or EBSD analyses were also similar. For example, the X-ray M-line of Nb (at 0.171 keV) was very close to the K-line for B (at 0.185 keV) [32], which needed a careful HPD. The SEM image of Fig. 6 shows a colony of Cr-rich rods formed on an Nb-rich precipitate. Quantification of the EDS spectra proved that the ratios of Nb:C in location

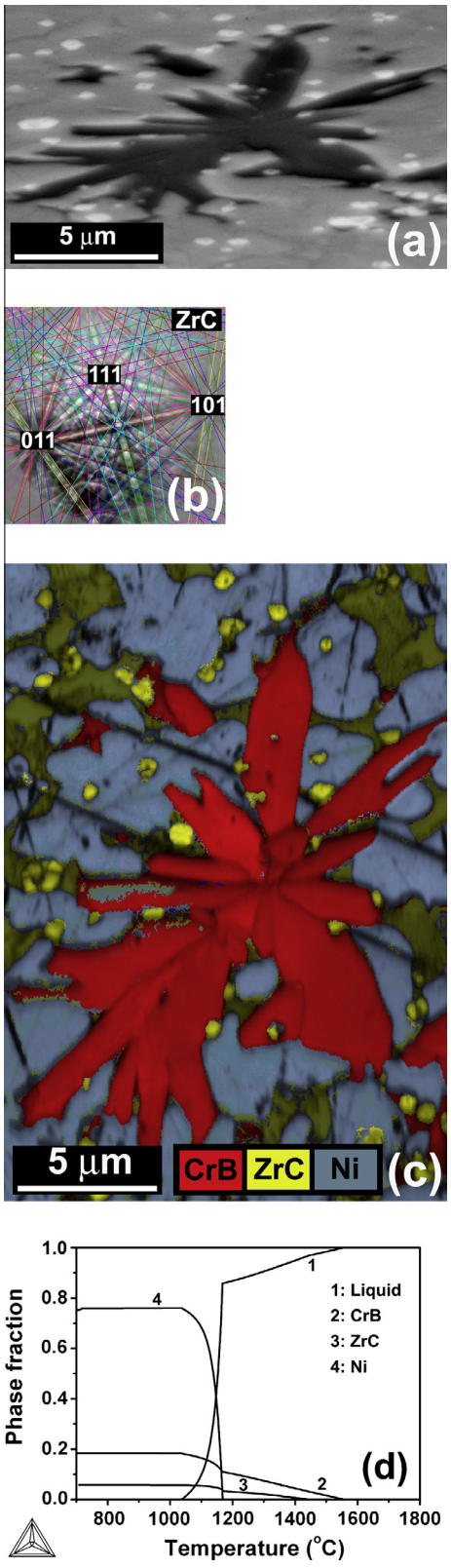

Fig. 5. (a) SEM–BSE image (tilted 70°) of the microstructure of coatings containing 5 wt.% Zr. (b) EBSD pattern obtained from the bright precipitates visible in (a) which could be indexed as ZrC. (c) The combined phase and image quality maps from the area in (a) showing the type of constituent phases. (d) Recalculated equilibrium phase fractions based on the phase identification results.

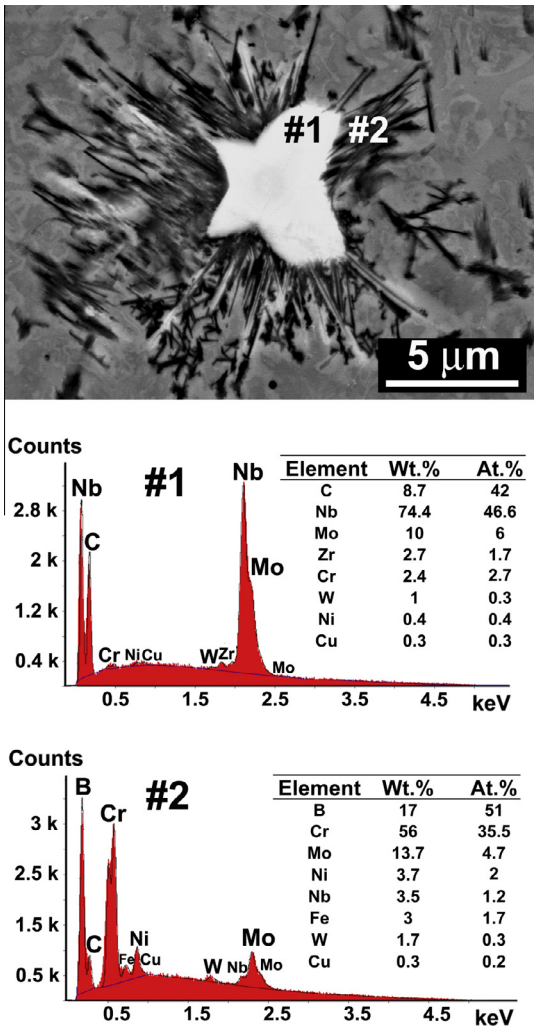

Fig. 6. EDS quantitative analysis of Nb- and Cr-rich precipitates labeled as #1 and #2, respectively, in the SEM–BSE image.

#1 and of Cr:B in location #2 were both close to unity. Hence, the Nb-rich and Cr-rich precipitates were expected to be of NbC and CrB type, as confirmed later by EBSD data.

With the same considerations as in Section 4.2.1, EBSD patterns from Nb carbide precipitate were indexed as NbC (Fig. 7b). The phase constitution in the intended area was determined by EBSD scanning, as shown in the phase map of Fig. 7c. The interdendritic regions of the Nb-modified deposits were usually indexed as NbC, which was also an artifact caused by the fine Ni layers in the eutectic areas and the crystallographic similarity of Ni and NbC (cubic crystals, $(O_h)[m3m]$ symmetry point groups, lattice parameters of 0.356 nm for Ni and 0.447 nm for NbC).

4.3. Variations of hardness

Ni–Cr–B–Si–C alloys are intended for wear applications [3,4]. Consequently, refinement of their microstructure ideally should be done while preserving their high hardness.

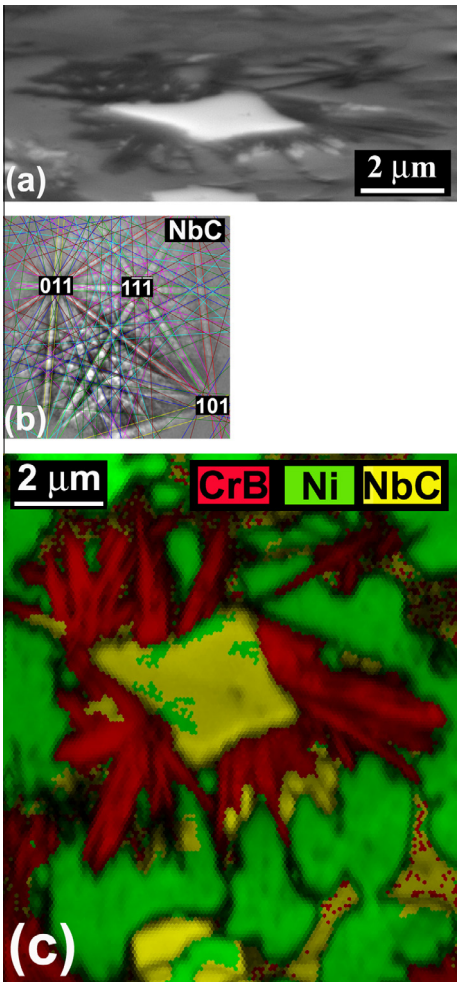

Fig. 7. (a) SEM–BSE image (tilted 70°) of the microstructure of Nb-modified coatings. (b) EBSD pattern obtained from the bright carbide precipitate in (a) which could be indexed as NbC. (c) The phase map (combined with image quality map) showing the type of constituent phases for the area in (a).

Fig. 8 shows the hardness of the Zr-modified and Nb-modified microstructures shown in Figs. 2b (Colmonoy 69 + 5 wt.% Zr) and 3b (Colmonoy 69 + 4 wt.% Nb). The hardness of the original alloy was in the range of 700–900 HV [33]. Hence, the goal of refining the microstructural without deteriorating the hardness was largely achieved for the Nb-modified deposits. However, the addition of Zr reduced the hardness of the original alloy. In previous works, both increase (with Ta addition [10]) and decrease (with Ti [9] or V additions [5,6]) in the hardness of the original Ni–Cr–B–Si–C alloys have been reported. The hardness of Ni–Cr–B–Si–C alloys is controlled by the type and quantity of hard precipitates, such as borides and carbides, and the eutectics [33,34]. An increase or decrease in the hardness of Ni–Cr–B–Si–C alloys as a result of Ta, Ti, V, Zr or Nb additions could be explained by the way these elements influence the eutectic reactions. Otherwise, all of these elements produce very hard carbides and borides [16,17], which should normally increase the overall hardness.

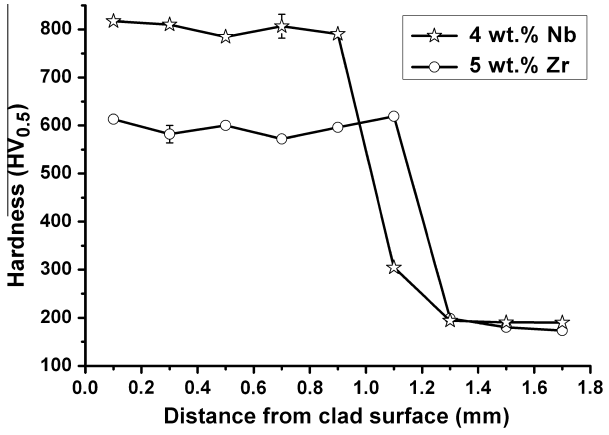

Fig. 8. Hardness graphs for the deposits modified by 4 wt.% Nb or 5 wt.% Zr additions.

5. Discussions

It was shown that the proposed procedure to select refining elements based on their ability to form precipitates at high temperatures which could remain as independent phases and act as heterogeneous nucleation sites was able to refine the microstructure of Ni–Cr–B–Si–C alloys. Based on the phase formation reactions and the microstructural evolutions in Nb-, Zr- and V-modified [6] deposits, the set of proposed rules in Section 2 can be further analyzed.

According to the ΔG_f data [14,17], it was expected that new borides would form upon the addition of Zr or Nb to the original alloy, but none were formed. It should be noted that the reported ΔG_f data are usually measured or calculated for reactions in which pure elements react or a single chemical reaction occurs to form that compound [14]. Formation of the same compounds may not necessarily happen in a multi-component system as they may not contribute to bringing the free energy of the whole system to its minimum. From this point of view, the application of thermodynamic calculation software to consider competing reactions in the multi-component system is essential. An example of this was shown for the Nb-modified alloy, in which the type and sequence of phase formations (Fig. 1) were predicted by Thermo-Calc® simulations with reasonable precision. Nevertheless, such simulations could not account for the non-thermodynamic effects, which could become dominant, especially in processes including rapid solidification, such as laser deposition. In other words, while ZrB_2 plus Cr_7C_3 was the most thermodynamically favorable set in the alloy modified by 5 wt.% of Zr (Fig. 1a and c), in reality the Zr and C content of the alloy precipitated as ZrC. Such a phase selection phenomenon was most probably nucleation controlled, as no borides were detected in the microstructure (Fig. 5c) or predicted by the recalculated phase formation sequence (Fig. 5d). In an alloy system with numerous phases, competition in the nucleation-controlled regime will be largely determined

by the relative magnitudes of ΔG^*, i.e. the energy barrier to heterogeneous nucleation, which can be represented as [35]

$$\Delta G^* = \frac{16\pi\gamma_{SL}^3 T_m^2 f(\theta)}{3L_f^2 \Delta T^2}$$

where ΔT is the undercooling of the liquid phase, γ_{SL} is the solid–liquid interface energy, T_m is the equilibrium melting point, L_f is the latent heat of phase formation and $f(\theta)$ is the nucleation potency factor of the heterogeneous site that depends on the wetting angle θ. It can be seen that ease of nucleation depends not only on the latent heat of phase formation (L_f or i.e. ΔG_f) but also on other parameters such as the solid–liquid interface energy and a suitable level of undercooling below the equilibrium melting temperature. Selection of the refining element based only on the ΔG_f values, as suggested before [5], ignores the fact that ΔG_f of a compound mostly shows the stability of that phase and not its ease of formation.

In an alloy system with multiple phase formation reactions, the sequence of phase formation should also be assessed. This is particularly important for the refinement process because an obvious prerequisite for an in situ formed nucleating agent is its high temperature of formation. The recalculated solidification sequence of the Zr-modified alloy as presented in Fig. 5d shows that ZrC started to form at more than 100 °C after CrB, by which stage the nucleation of CrB would have been largely completed. As a result, ZrC particles could not act as nucleation sites and hence the addition of Zr did not induce any microstructural refinement. A similar phenomenon was observed for V-modified alloys, in which VC precipitates formed at lower temperatures on (Cr,V)B rods and consequently could not function as nucleating agents [6].

Apart from the thermodynamic possibility of spontaneous precipitation as well as ease and temperature of formation, solid-state interaction between the nucleant and the Cr borides nucleating on them may influence the final phase constitution of the system. This effect was characterized in detail for the interaction between VB and CrB in the V-modified system [6]. As expected from the size factors and the differences in the crystal structures of the Zr- and Nb-rich phases, strong segregation happened between CrB and ZrC or NbC (Figs. 4 and 6).

Although the methodology and the rules proposed thus far could explain a good deal about the selection of effective alloying elements for microstructural refinement of Ni–Cr–B–Si–C alloys, they need further elaboration in certain areas. The first requirement is to explain the role of kinetic effects in the phase selection processes, as briefly mentioned above. This is pivotal when the additional element can go through multiple precipitation reactions, especially in rapid solidification processes such as laser deposition. The second point is to understand the nucleation mechanism in the refined microstructure of Nb-modified alloys. In the current work, the nucleating capability of NbC was attributed to its high temperature of formation and its lack of solubility in CrB, which enabled it to remain as an independent phase. However, such an argument ignores the fact that a good nucleating agent should fulfill more conditions than just being physically available at the right temperature. For example, the surface energy between a heterogeneous nucleation site and a solid crystal should be lower than the surface energy between a heterogeneous nucleation site and the melt [28]. Such a condition is in turn controlled by factors including the lattice disregistry and orientation relationship between the nucleant and the growing crystal and the chemical nature of the surface layer on the nucleant [36].

As the refined microstructure of Nb-modified hardfacing alloys possesses the same level of hardness as the coatings deposited from the original alloy (Colmonoy 69), they can be used in further research to investigate if the idea of microstructural refinement is a viable toughening mechanism for rapidly solidified Ni–Cr–B–Si–C hardfacing alloys.

6. Conclusions

In this research, the idea of reducing the structural scale of Cr-rich precipitates in Ni–Cr–B–Si–C hardfacing alloys by producing in situ formed nucleation agents via the controlled addition of refining elements was explored. It was proposed that the refining element should be able to spontaneously produce precipitates at high temperatures with little solid solubility in their Cr-rich counterparts. Based on the proposed rules, additions of Zr and Nb were done during laser deposition of a commercial Ni–Cr–B–Si–C alloy powder. While no microstructural refinement occurred in Zr-modified deposits, Nb addition could significantly refine the scale of Cr boride precipitates because of nucleation of CrB rods on NbC precipitates. The lack of microstructural refinement in Zr-modified coatings could be explained based on Thermo-Calc® simulations, which showed that ZrC formed at much lower temperatures in comparison to CrB. The Nb-modified deposits, with their refined microstructure, could be used to study the viability of microstructural refinement as a toughening mechanism for hardfacing alloy systems such as Ni–Cr–B–Si–C.

Acknowledgements

This research was carried out under Project Number MC7.06259 in the framework of the Research Program of the Materials innovation institute M2i (www.m2i.nl). The Wall Colmonoy Ltd. (The UK) is acknowledged for providing Colmonoy 69 powders.

References

[1] Ajao JA. J Miner Mater Charact Eng 2010;9:133.
[2] Conde A, Zubiri F, De Damborenea YJ. Mater Sci Eng A 2002;334:233.
[3] Miguel JM, Guilemany JM, Vizcaino S. Tribol Int 2003;36:181.

[4] Fernández E, Cadenas M, González R, Navas C, Fernández R, Damborenea JD. Wear 2005;259:870.
[5] Wang DS, Liang EJ, Chao MJ, Yuan B. Surf Coat Technol 2008;202:1371.
[6] Hemmati I, Rao JC, Ocelík V, Hosson JTMD. J Mater Sci 2013;48:3315.
[7] Huang Y, Zeng X. Appl Surf Sci 2010;256:5985.
[8] Zhou S, Dai X, Zheng H. Opt Laser Technol 2011;43:613.
[9] Chao M-J, Liang E-J. Surf Coat Technol 2004;179:265.
[10] Yu T, Deng Q, Dong G, Yang J. Appl Surf Sci 2011;257:5098.
[11] Yu T, Deng Q-L, Zhang W, Dong G, Yang J. J Shanghai Jiaotong Univ (Sci) 2012;46:1043.
[12] Knott JF. Fundamentals of fracture mechanics. London: Butterworth; 1973.
[13] Branagan DJ, Marshall MC, Meacham BE. Mater Sci Eng A 2006;428:116.
[14] Barin I. Thermochemical data of pure substances. 3rd ed. Weinheim: VCH; 1995.
[15] Cottrell A. Chemical bonding in transition metal carbides. London: Institute of Materials; 1995.
[16] Pierson HO. Handbook of refractory carbides and nitrides: properties, characteristics, processing, and applications. Park Ridge, NJ: Noyes Publications; 1996.
[17] Culter R. A. Engineering Properties of Borides, in: Samuel J. Schneider technical chairman (Ed.), Engineered Materials Handbook, Ceramics and glasses,, ASM International, USA, 1991;4 pp. 787–803.
[18] Mizutani U. Hume-Rothery rules for structurally complex alloy phases. Boca Raton, FL: CRC Press; 2011.
[19] Darken LS, Gurry RW. Physical chemistry of metals. New York: McGraw-Hill; 1953.
[20] Chelikowsky J. Phys Rev B 1979;19:686.
[21] Zhang YM, Yang S, Evans JRG. Acta Mater 2008;56:1094.
[22] Fedorov TF, Kuz'ma YB. Sov Powder Metall Metal Ceram 1965;4:234.
[23] Fedorov TF, Popova NM, Gorshkova LV, Skolozdra RV, Kuz'ma YB. Sov Powder Metall Metal Ceram 1968;7:193.
[24] Kuz'ma YB, Telegus VS, Kovalyk DA. Sov Powder Metall Metal Ceram 1969;8:403.
[25] Hugosson HW, Jansson U, Johansson B, Eriksson O. Chem Phys Lett 2001;333:444.
[26] Chen HM, Zheng F, Liu HS, Liu LB, Jin ZP. J Alloys Compd 2009;468:209.
[27] Tang Z, Kramer MJ, Akinc M. Intermetallics 2008;16:255.
[28] Dantzig JA, Rappaz M. Solidification. Lausanne: EPFL Press; 2009.
[29] Hemmati I, Rao JC, Ocelík V, De Hosson JTM. Microsc Microanal 2013;19:120.
[30] Toyserkani E, Corbin S, Khajepour A. Laser cladding. Boca Raton, FL: CRC Press; 2004.
[31] Hemmati I, Ocelík V, De Hosson JTM. Mater Lett 2012;84:69.
[32] Zschornack G. Handbook of X-ray data. New York: Springer; 2006.
[33] Hemmati I, Ocelík V, De Hosson JTM. WIT transactions on engineering sciences, vol. 71. Malta: WIT Press; 2011. p. 287–96.
[34] Tanaka K. US patent 4,404,049; 1983.
[35] Perepezko J, Brewer L, Schaefer R. Mater Sci Eng 1985;70:9.
[36] Murty BS, Kori SA, Chakraborty M. Int Mater Rev 2002;47:3.